ACS OMEGA

http://pubs.acs.org/journal/acsodf

Article

Binder Selection to Modify Hydrocarbon Cracking Properties of Zeolite-Containing Composites

Andres Carrasco Saavedra, Vladislav Timoshev, Mathias Hauck, Mehdi Hassan Nejad, Tung Thanh Dang, Xuan Hoan Vu, Markus Seifert, Oliver Busse, and Jan J. Weigand*

Cite This: *ACS Omega* 2022, 7, 16430−16441

Read Online

ACCESS | Metrics & More | Article Recommendations | Supporting Information

ABSTRACT: Activity, selectivity, and deactivation behavior of catalyst materials determine their efficiency in hydrocarbon conversion processes. For hydrocarbon cracking, the industrial catalyst is an important parameter in reaction technology to produce valuable compounds, *e.g.*, light olefins (C_3−C_5) and gasoline from crude oil fractions with high molecular weight (C_{16+}). One strategy to enhance the catalytic activity for precracking is increasing the matrix activity, which depends on the used binder and additives. In this work, three binders (water glass, aluminum chloride, and a mixture of colloidal silica with aluminum dihydrogen phosphate) were used in combination with active zeolite Y, kaolin as filler, and ZSM-5 as additive to produce composite materials. Specific surface area and surface acidity measurements were combined with catalytic testing of the formulated samples in order to find the relation between the catalyst morphology and its activity. In addition, constraint index was used as a control parameter for the determination of the shape-selective properties and their correlation with the catalytic activity. The results show that the binders determine the porosity of the matrix and so the accessibility to zeolite pores and active sites. Matrixes with low porosity and activity enhance coke production and deactivate faster than matrixes with mesopores. Furthermore, ZSM-5 modifies the individual morphological and catalytic effects of the binders. Everything considered, the small crystals of ZSM-5 together with mesopores increase the olefins yield, reduce coking, and therefore enhance the performance of the final grain.

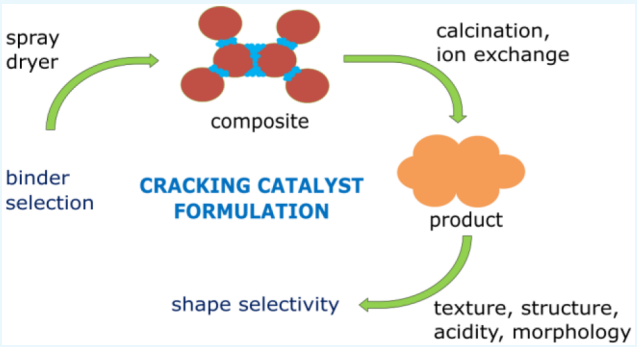

1. INTRODUCTION

The increasing demand for high-quality petrochemical products and fuels represents a challenge for oil refineries around the world. The use of low-quality feedstocks requires the improvement of the existing processes for the production of valuable products, *e.g.*, olefins for petrochemistry. In this context, catalytic cracking has become an important process, and the change of feedstock requires a flexible adaptation of the catalyst properties to ensure a good performance.[1−3] Therefore, different catalytic performance tests of these materials are important for the optimization of the cracking process.[4] Cracking catalysts are typically composite materials, which roughly consist of a zeolite such as zeolite Y as active material, a matrix, and additives. In this context, the matrix could be defined as the combination of fillers with binders.[5] An example for additive is ZSM-5 and kaolin for filler.[6] However, the binders applied for the manufacture of these catalysts are diverse and possess different properties. The selection of the components defines the catalytic behavior of the material as well as the resistance against fouling, poisoning, and certain mechanical and hydrothermal deactivation.[7] One important property is the catalytic activity, which is defined as the capacity of the catalyst to speed up the rate of a reaction.[8] This enhancement comes mainly from acidic zeolite components. Nevertheless, the presence of other active materials in the matrix, *e.g.*, acidic alumina binders, can increase the activity of the catalyst as well.[9] Another important property is the selectivity, which is mainly defined by the type of zeolite (pore structures), the activity of the matrix, and their interplay during hydrocarbon conversion. On the one hand, zeolite pores allow the passage and contact to active sites for specific molecules by shape selection. This phenomenon can be quantified through the constraint index,[10] which is defined as the relation between the conversion of two reactants with different molecular structure (3-methylpentane and *n*-hexane). On the other hand, the presence of a matrix can partially block the pores of the zeolite, which can reduce the catalyst activity. It is important to remember that mass transport phenomena can dominate the

Received: January 21, 2022
Accepted: February 28, 2022
Published: May 4, 2022

https://doi.org/10.1021/acsomega.2c00446
ACS Omega 2022, 7, 16430−16441

rates in catalytic processes. Adsorption and pore diffusion can limit the effectiveness of a catalyst. Therefore, the pore size distribution and the specific surface area are important parameters to consider in the evaluation of the catalyst. In addition, active matrixes can support precracking of molecules, allowing the contact of smaller molecules with the zeolite pores.[11]

This work focuses on the analysis of the mentioned effects of the binder on shape-selective catalyst properties. The morphological contribution of the matrix to the catalytic properties of the composite is quantified in the context of an additive ZSM-5 and different binders. For quantification of a material's characteristics, a detailed analysis of the surface, morphology, and acidity is coupled with constraint index measurements. Finally, the interplay between shape selectivity and the solid-state properties of the final composite grains follows from a detailed product analysis during hexane cracking reaction.

2. MATERIALS AND METHODS

2.1. Utilized Raw Materials. The materials utilized for the formulation and characterization are commercial zeolite CBV 400 by Zeolyst (zeolite Y as HY, $SiO_2/Al_2O_3 = 5.1$), CBV 5524G by Zeolyst (NH_4-ZSM-5, $SiO_2/Al_2O_3 = 50$), and kaolin by Sigma-Aldrich. As binders, sodium metasilicate (water glass) by Merck (27 wt % SiO_2; 8 wt % Na_2O), hydrated aluminum chloride by Alfa Aesar (99 wt % $AlCl_3 \cdot 6H_2O$), and aluminum phosphate monobasic purum (95 wt %) by Sigma-Aldrich were used together with LUDOX HS-40 (40 wt % SiO_2; mass ratio SiO_2/Na_2O: 95/1) by Sigma-Aldrich. In addition, hydrochloric acid (37%) from BDH Chemicals was added to control the pH value of water glass slurries. Moreover, ammonium nitrate (99 wt %) from Grüssing was used for post-treatment of the samples by ion exchange. Finally, concentrated hydrochloric acid and nitric acid (69 vol % supra-quality) from Carl Roth, hydrofluoric acid (40 vol %) from Merck, and boric acid (99.995 wt %) by Alfa Aesar were used in the microwave-assisted dissolution procedure for elementary analysis.

2.2. Sample Preparation. Before the preparation, NH_4-ZSM-5 was heated to 500 °C for 12 h in air flow of 100 L h^{-1} to obtain H-ZSM-5. The preparation process for the samples comprises the slurry preparation, formulation, and post-treatment of the products. For the slurry preparation, the binders were dissolved in water to form a solution and stirred for 10 min. Only in the case of water glass, the binder was diluted in water to 2.7 wt % and the pH value was adjusted with HCl (8 M) to pH 3. At this point, the other catalyst components (zeolites, kaolin) were added to the mixture, and the mixture was stirred with a speed of at least 900 rpm. The produced slurry was fed to a spray dryer B290 advanced from Büchi with a drying inlet temperature of 210 °C and a volumetric gas-to-liquid ratio of 427 (liquid flow of 1.26 L h^{-1}). Afterward, the drying product was calcined at 650 °C for 8 h in air flow. Only in the case of water glass, the product was washed and stirred with water (10 mL of water per gram of product) at room temperature for 1 h in order to remove soluble sodium species from the particles prior to the calcination.

After the calcination, the samples were treated with ammonium nitrate solution (5 wt %, ion exchange) at 60 °C in two cycles. Filtered solid product was afterward washed with water and dried at 120 °C for 12 h. Dried samples were calcined at 550 °C for 5 h in air flow. Finally, the samples were pressed and sieved to produce grains with a particle size between 315 and 400 μm for catalytic testing. The nomenclature and composition of the samples prepared for this study are presented in Table 1.

Table 1. Composition of Slurries and Samples for Catalyst Formulation with Silica Binder, Alumina Binder, and Phosphate-Silicate Binder[a]

sample name	S	S-Z	A	A-Z	PS	PS-Z
binder name	water glass		aluminum chloride		aluminum phosphate + colloidal silica[a]	
binder components	sodium metasilicate		$AlCl_3$		$Al(H_2PO_4)_3$: 30.2 wt % SiO_2: 69.8 wt %	
total amount of solids in slurry (wt %)	10	10	10	10	30	30
amount of HY in solids (wt %)	44.4	44.4	44.4	44.4	44.4	44.4
amount of binder in solids (wt %)	22.2	22.2	22.2	22.2	22.2	22.2
amount of kaolin in solids (wt %)	33.3	28.3	33.3	28.3	33.3	28.3
amount of ZSM-5 in solids (wt %)	0.0	5.0	0.0	5.0	0.0	5.0

[a]Use of (basic) colloidal silica to adjust pH value to >2 of acidic phosphate containing binder; prevention of corrosion in the spray drying device as reported earlier.[12] -Z denotes addition of ZSM-5.

2.3. Sample Characterization. Specific surface area of the samples was determined with a Surfer gas adsorption porosimeter by Thermo Scientific. The samples were preheated to 250 °C and calcined in vacuum for 8 h. The physisorption results were analyzed using the BET theory,[13] and the porosity of the particle was determined through the BJH method.[14,15] The range of the pore diameter determined by the BJH method is 4−10 nm. In addition, temperature-programmed ammonia desorption (TPAD) was done with a TPDRO 1100 instrument (Thermo Scientific) equipped with a thermal conductivity detector (TCD). The measurement preparation consisted of the drying of 150 mg of sample under flowing argon at 250 °C and a cooling to 120 °C. Afterward, ammonia adsorption was performed for 10 min, and desorption was done under helium flow for 3 h and heating to 550 °C for 1 h with a heating rate of 10 K/min. The amount of desorbed ammonia was calculated by integrating signals using device internal calibration. Strong acid sites were calculated using signal area from 20 (315 °C) to 45 min (550 °C) of measurement time. Moreover, XRD patterns of the samples were measured on a STADI P X-ray powder diffractometer from STOE. The transmission measurements of the solid samples were realized with Cu Kα_1 radiation at room temperature in the 2θ range between 5° and 90°. For the measurement, the samples were fixed between two X-ray amorphous adhesive strips. Furthermore, scanning electron microscopy (SEM) and energy-dispersive X-ray spectroscopy (EDX) analysis were performed on a scanning electron microscope SU8020 (HITACHI) equipped with an energy-dispersive X-ray spectrometer X-MaxN (OXFORD Instrument). For SEM, an electron beam voltage of 2 kV was used to reach a magnification factor between 2 500 and 10 000. The samples were dried at 60 °C and ambient pressure overnight in an oven and afterward at room temperature and under reduced pressure (<70 mbar) for 48 h in a desiccator prior to the measurement. For EDX element mapping, an acceleration voltage of 15 kV was used at a magnification of 2500. In addition,

https://doi.org/10.1021/acsomega.2c00446
ACS Omega 2022, 7, 16430−16441

Table 2. Determination of Si, Al, Na, Fe, and P by ICP-OES for Composites

sample name	S	S-Z	A	A-Z	PS	PS-Z
Si (wt %)	33.97 ± 0.03	34.16 ± 0.15	25.98 ± 0.12	25.88 ± 0.82	31.15 ± 0.12	33.68 ± 0.29
Al (wt %)	12.86 ± 0.06	12.36 ± 0.28	20.74 ± 0.08	19.29 ± 0.08	12.52 ± 0.03	10.75 ± 0.27
Na (wt %)	0.39 ± 0.01	0.38 ± 0.01	0.44 ± 0.01	0.39 ± 0.01	0.34 ± 0.01	0.27 ± 0.01
Fe (wt %)	0.21 ± 0.01	0.19 ± 0.03	0.22 ± 0.01	0.20 ± 0.15	0.19 ± 0.00	0.13 ± 0.00
P (wt %)	<LOQ[a]	<LOQ[a]	<LOQ[a]	<LOQ[a]	3.2 ± 0.04	3.2 ± 0.04

[a]LOQ (limit of quantification).

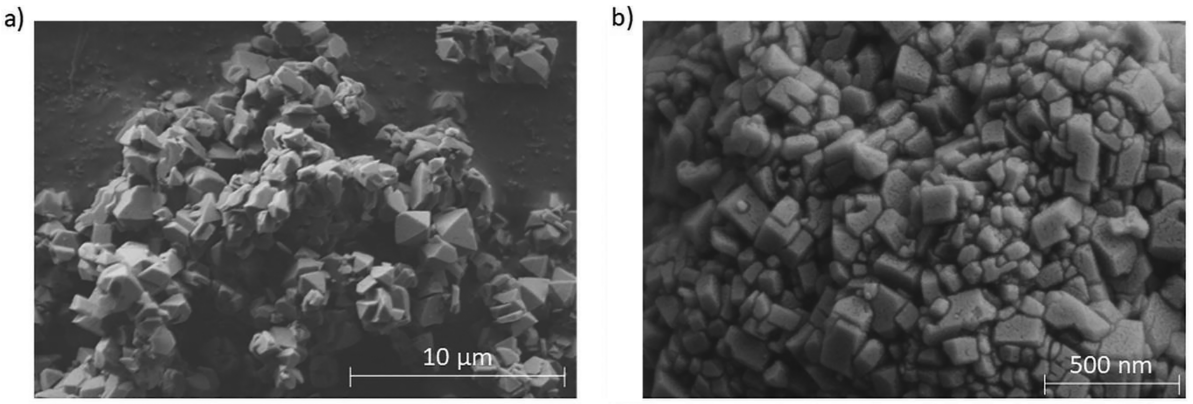

Figure 1. SEM pictures of commercial (a) HY (magnification: ×10 000) and (b) ZSM-5 zeolite (magnification: ×60 000).

epoxy resin was used to ensure a plain surface after sawing and polishing. In order to avoid any charge-up and chemical alteration during the measurements, the sample's surface was coated with gold in an automatic rotary-pump coating system (Quorum Q150R ES).

Inductively coupled plasma optical emission spectrometry (ICP-OES) was done for the determination of the content of Si, Al, Na, Fe, and P in the composites using a PerkinElmer Optima 2000DV. The wavelengths used for this analysis were 237.313, 394.401, and 396.156 nm for Al; 588.995 and 589.592 nm for Na; 212.412 and 251.611 nm for Si; 213.617 and 214.914 nm for P; and 238.204 and 259.939 nm for Fe. Prior to the ICP-OES measurement, a mixture of HCl, HNO_3, HF, and for quenching H_3BO_3 was used together with a microwave CEM Mars 6 instrument to dissolve the samples. Furthermore, particle size distribution of all powders in water was measured and analyzed through laser scattering with a Bettersizer S3-Plus by 3P-Instruments using the Mie theory. The samples were measured under ultrasonic conditions (60W). Thermogravimetric analysis was done with a TG50 by Mettler Toledo for coke determination. The used catalyst samples were heated from 35 to 850 °C in air flow, with a heating rate of 3 K min^{-1} and 10 K min^{-1} (see Figure S4).

2.4. Characterization of Pore Accessibility and Constraint Index. Catalytic behavior during cracking of hexane mixtures is used as a tool to characterize shape-selective material properties and site accessibility by the pore access of linear versus branched hydrocarbons. It is summarized as the constraint index (CI) test method.[16] CI was calculated with the following equation:

$$\mathrm{CI} = \frac{\log(1 - X_n)}{\log(1 - X_{\mathrm{iso}})} \quad (1)$$

where CI is the constraint index, X_n the conversion of *n*-hexane (linear isomer), and X_{iso} the conversion of 3-methylpentane (branched isomer).

Samples were pelleted at 3 MPa, grinded, and sieved to obtain particle sizes in the range of 315−400 μm. A 4 g portion of the dry sample was tested in a stainless-steel tubular reactor between quartz wool support. The sample was heated to 350 °C in the reactor with a flow of nitrogen (6 L h^{-1}, GHSV = 830 h^{-1}) and calcined for 4 h. Afterward, the reactor was heated to 500 °C, and a mixture of 50 mol % *n*-hexane and 50 mol % 3-methylpentane was fed by a syringe pump with 5 mL h^{-1} flow rate (LHSV = 0.7 h^{-1}) in the reactor. Gas phases were analyzed during 6 h time on stream (TOS) by a Clarus 590 GC from PerkinElmer equipped with an HP-1 100 m column and a flame ionization detector (FID) using a detailed hydrocarbon analysis (DHA) according to ASTM Standard D 6730-19.[17] All measurements were performed as double-determination.

3. RESULTS AND DISCUSSION

3.1. Comparison of Composite Materials with Different Binders. The contents of silicon, aluminum, sodium, iron, and phosphorus of the formulated composites were determined by ICP-OES (oxygen was not determined). The aluminum content changed depending on the used binder and additive. In the case of the formulations with aluminum chloride, the concentration of aluminum was the highest. In addition, minor amounts of sodium were identified in all composites, which resulted from residual sodium in kaolin and silica-containing binders, even after ion exchange after spray drying and calcination. Moreover, iron impurities were observed in the formulation, which originated from kaolin (0.57 wt % of iron). Finally, a reduction of aluminum, iron, and sodium content was observed in the formulations with ZSM-5. This is expected, because the kaolin amount is reduced in formulations with ZSM-5. The results are shown in Table 2.

Composite materials of HY as well as ZSM-5, kaolin, and different binders were prepared, analyzed, and catalytically tested for hexane cracking. In order to identify the active components of the composite in the SEM pictures, the used

https://doi.org/10.1021/acsomega.2c00446
ACS Omega 2022, 7, 16430−16441

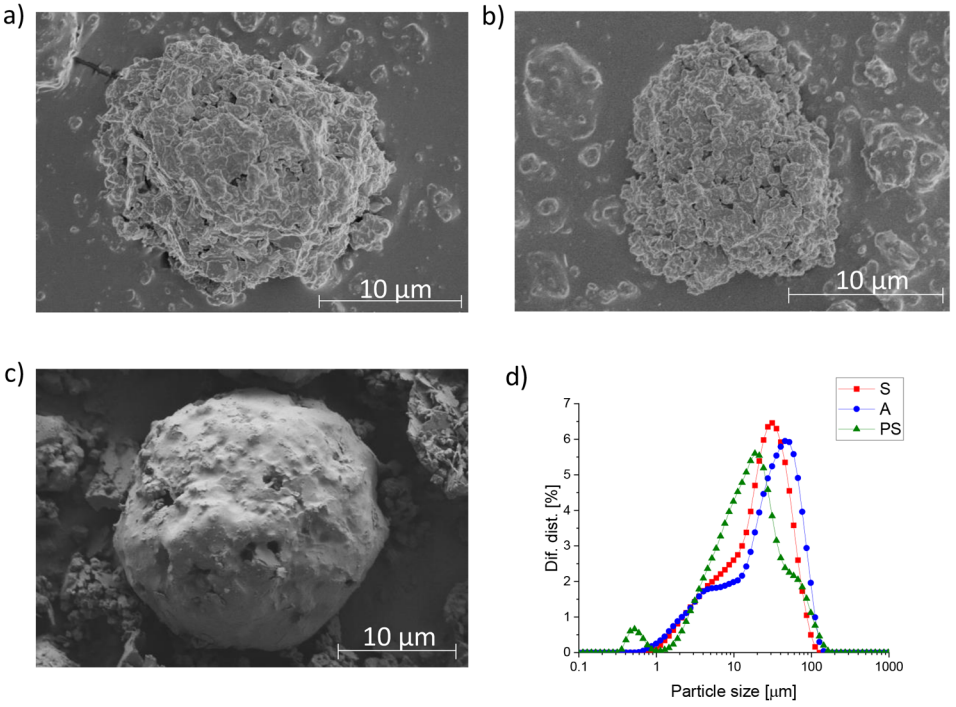

Figure 2. SEM pictures of composites of HY and kaolin with (a) water glass (S), (b) aluminum chloride (A), and (c) AlPO binder (PS); magnification factor: ×3500. (d) Particle size distribution of composites.

Scheme 1. Agglomeration Mechanism of Binders in Cracking Catalyst Formulation[a]

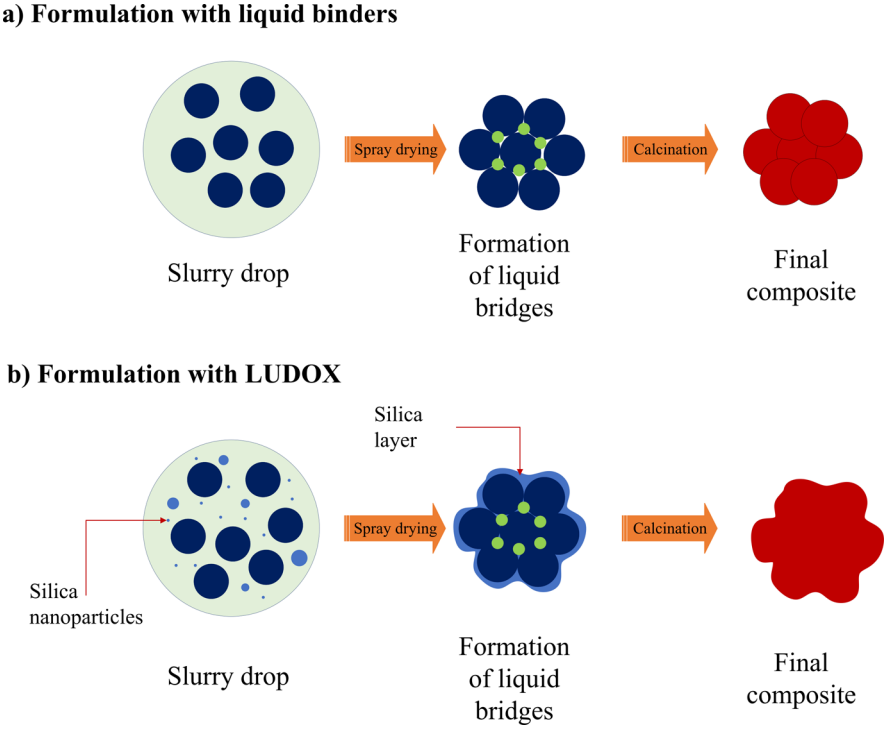

[a](a) Formation of liquid bridges for interparticle binding and (b) formation of liquid bridges and particles layers for interparticle binding and formation of an outer shell/crust.

zeolites of the formulations (zeolite Y and ZSM-5) were analyzed independently as parent materials. Zeolite Y possesses an orthorhombic structure (see Figure 1a). Crystals up to 2 μm were identified in the SEM pictures. The crystals of ZSM-5 (see Figure 1b) are rectangular and smaller (200 nm). Crystal size, particle size, and interparticle volume strongly influence textural properties.

SEM pictures of the composite particles formed with zeolite Y, kaolin, and binders are shown in Figure 2. A comparison of Figures 1 and 2 reveals that composite particles are formed by

https://doi.org/10.1021/acsomega.2c00446
ACS Omega 2022, 7, 16430−16441

the agglomeration of different smaller compounds. However, the arrangement of the particles and the structure of these differ. The samples S and A show a surface with more visible pores because of the agglomeration of particles of size over 2 μm by liquid bridges. In this case, the binding comes from the precipitation of the binder from the liquid phase.[12,18] However, this was not observed in the sample PS, where silica nanoparticles from LUDOX are present in the formulation. These nanoparticles can agglomerate faster to other bigger particles and can cover all their surface. Consequently, it produces a silica layer over the composite surface. Scheme 1 depicts the unusual behavior compared to other binder processes. The properties of these layers are analyzed in detail in Section 3.2.

The laser scattering results of the samples (see Figure 2d) show a nonhomogeneous distribution in all cases with formed agglomerates. The average particle size of the composites is in the range of the spray nozzle diameter (approximately 20−25 μm), as listed in Table 3. In addition, for sample PS there is a

Table 3. Textural and Acidic Properties of Composites

sample	D_{50}[a] (μm)	S_{BET}[b] ($m^2 g^{-1}$)	S_{meso}[c] ($m^2 g^{-1}$)	V_{total} ($cm^3 g^{-1}$)	desorbed NH_3 (μmol(NH_3) g^{-1}) strong	total
S	21.5	348	30	0.190	937	1428
A	26.7	326	51	0.230	1069	1568
PS	21.7	264	53	0.185	785	1255
S-Z	17.5	299	31	0.176	680	1148
A-Z	22.1	368	69	0.287	965	1393
PS-Z	24.9	287	48	0.184	836	1261

[a]D_{50} = maximum particle size of 50% smallest particles in a sample from Mie theory.[25,26] [b]S_{BET} = specific surface area from BET theory.[21] [c]S_{meso} = surface area of mesopores from BJH theory.[14]

formation of particles below 1 μm. This implies the agglomeration among binder particles (silica nanoparticles and aluminum phosphate) occurs independently in a first instance. This occurs because of the higher agglomeration rate of the silica nanoparticles in the soluble phosphate binder. With ongoing agglomeration, the particles grow and the agglomeration rate decreases as slurry concentration and surface/volume ratio of the agglomerates decrease until the binding of silica particles stops.

In parallel, powder diffraction patterns were prepared for the characterization of different crystalline phases within the final composites (see Figure 3). In comparison with the references, only the reflections of the diffraction patterns of zeolite Y are identified in all products, which implies that the matrix components remain almost completely amorphous within the limits of XRD sensitivity. The reference for this analysis was the commercial HY CBV 400 by Zeolyst, which is comparable with references from the literature[19] (see Figure S1). As an exception, the pattern of sample PS shows lower intensity of the signal, which indicates structural degradation during the preparation procedure.

Results from nitrogen physisorption and temperature-programmed adsorption of ammonia in Figure 4 also confirm deviating physicochemical properties between zeolites and other compounds. The observed isotherms are of type II, which is typical for samples with micropores as well as larger macropores of nonuniform sizes.[20,21] In the case of samples with ACH

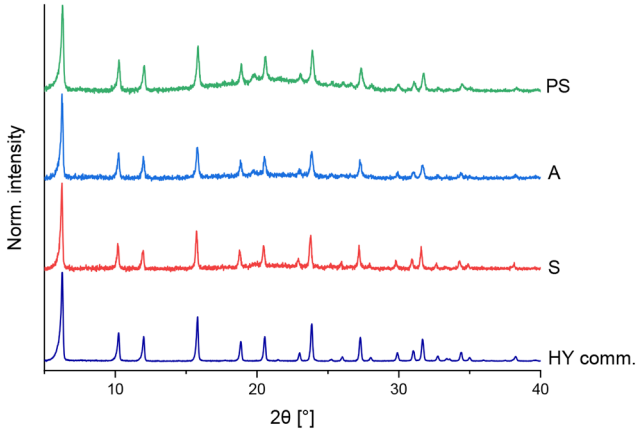

Figure 3. XRD patterns of composites with HY, kaolin, and binders: water glass (S), aluminum chloride (A), and aluminum phosphate incl. colloidal silica (PS). Reference for zeolite Y: HY commercial product from Zeolyst.

binder (samples A), there is a transition to type IV(a) isotherms, which indicates the presence of smaller macropores or even mesopores.[21] For further information, see Figure S2. Furthermore, a quantification of the mesopore size distribution through the BJH method shows that the composites have a higher amount of mesopores than zeolite Y (see Figure 4a). A pore signal at 3 nm is observed for the samples S and PS, which is attributed to the limited capillary effect for nitrogen in small mesopores, so-called tensile strength effect.[22,23] This indicates the presence of even smaller pores at the transition between zeolite pores and mesopores. In general, the adsorption and desorption curves show a very small hysteresis, which implies the dominance of small micropores over mesopores in the system. However, sample A shows a reduced tensile strength effect, which is attributed to its higher mesopore volume (see Table 3), higher adsorption volume, and a wider hysteresis than the other samples (see Figure 4a). The increment of the mesopore amount in sample A can be caused by the acidity of the alumina binders, which slightly leaches the solid components during the formulation (kaolin and zeolite) and produces higher amount of bigger mesopores. In addition, a locally distributed agglomeration of the alumina compared to silica binder also contributes to a wider size-distribution of mesopores by the interconnection of the solid components in the grain and partial filling of interparticle voids.[12]

Surface acidity was determined by TPAD (see Figure 4b). The samples S and A show a similar behavior for ammonia desorption. Even though the alumina binder is acidic, there was a slight increment of ammonia desorption results in the composite. This can be attributed to the low density of active sites of the alumina binder. In addition, the sample PS shows lower ammonia desorption than the other formulations, because phosphorus from the binder tends to deactivate the active acid sites of both zeolites.[24] In addition, the sample has less pore volume than the others, which reduces the contact of the ammonia with the acid sites.

The obtained TPAD results are a first indication for the hydrocarbon cracking properties of the composites, because the number and strength of acid sites of the zeolite are related to its activity. However, the acidity determination by this method has some limitations. According to Gorte et al.,[27] ammonia chemisorption could not be accurate to determine the

https://doi.org/10.1021/acsomega.2c00446
ACS Omega 2022, 7, 16430−16441

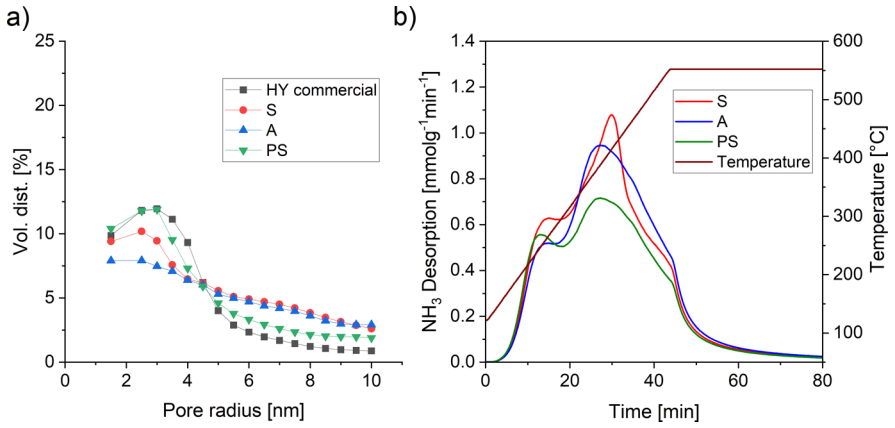

Figure 4. (a) Pore size distribution (BJH method) and (b) TPAD results of formulated composites with each binder.

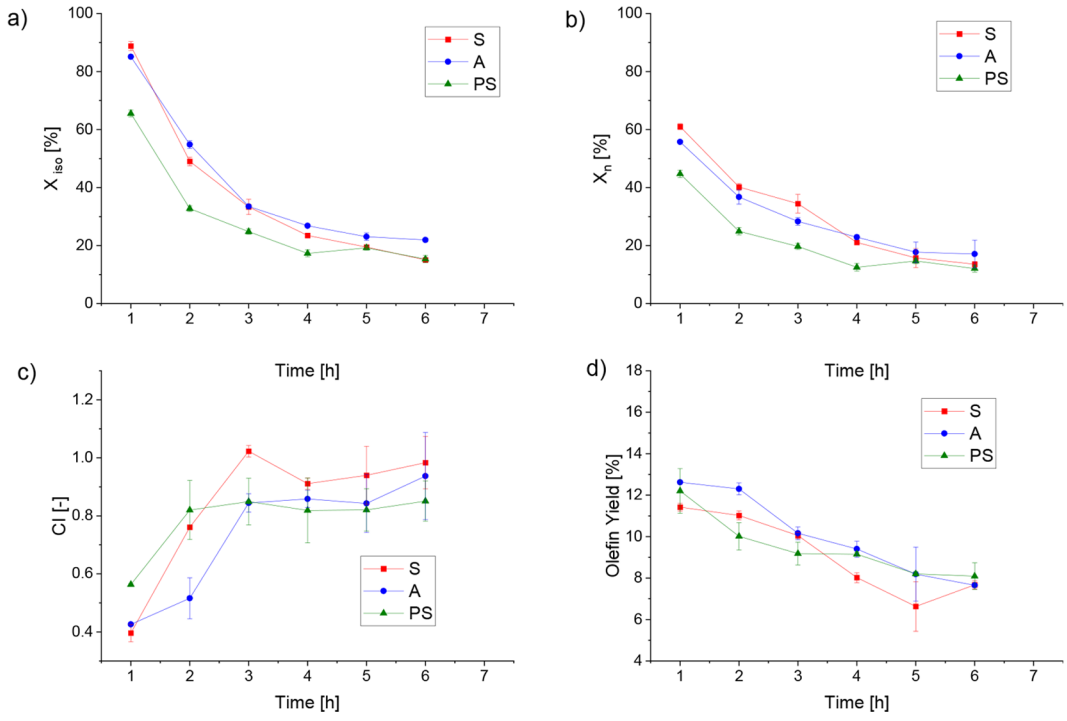

Figure 5. Conversion of (a) 3-methylpentane and (b) *n*-hexane for formulations with different binders; (c) constraint index and (d) olefin yield of formulated composite materials with different binders.

temperature of strong acidity because of further parameters associated with the ammonia adsorption, *e.g.*, site density, particle and crystal size, *etc.* In addition, ammonia adsorption is not selective for Brønsted acid sites. In that case, it is recommended to use protonated bases, such as pyridine, as adsorbents or ^{13}P NMR spectroscopy of adsorbed trimethyl phosphane(oxide) for the determination of Lewis acid sites.[28] Nevertheless, this limitation does not affect the analysis of this work because it is not its focus to determine the type of acid sites of the samples. A further limitation of TPAD is that adsorption enthalpy does not directly correlate to the activity of the catalyst, because the adsorption of ammonia could be influenced by interaction of ammonia with other species which do not participate in the reaction as well as confinement effects within the particle. Therefore, the amount of adsorbed ammonia obtained during the measurement depends not only on the amount of acid sites in the composite but also on their accessibility. This aspect has already been discussed by the surface description from physisorption experiments (see Table 3). Higher micro- and mesopore surface area for A and A-Z correlate with higher amounts of desorbed ammonia. The resulting impact on the selective hydrocarbon cracking of hexanes will be discussed by the constraint index determination.

However, some undesired interactions between binders and zeolite can occur during the formulation of the catalyst (see Figure S3). In the case of water glass, sodium can re-exchange protons of zeolite Y, which reduces its acidity.[7,9,29−32] In the case of aluminum chloride, aluminum species can adhere to the acid sites of the zeolite, which deactivates this material.[11,33−37] Furthermore, phosphate species from the aluminum phosphate binder can interact with the aluminum inside and outside the zeolite pore system and reduce its activity.[24,38,39] From XRD, TPAD, and physisorption experiments of the sample PS, the mentioned interaction between the phosphorus containing matrix and the zeolite phase is confirmed, which can be an indicative of partial destruction of zeolite Y crystals because of

https://doi.org/10.1021/acsomega.2c00446
ACS Omega 2022, 7, 16430−16441

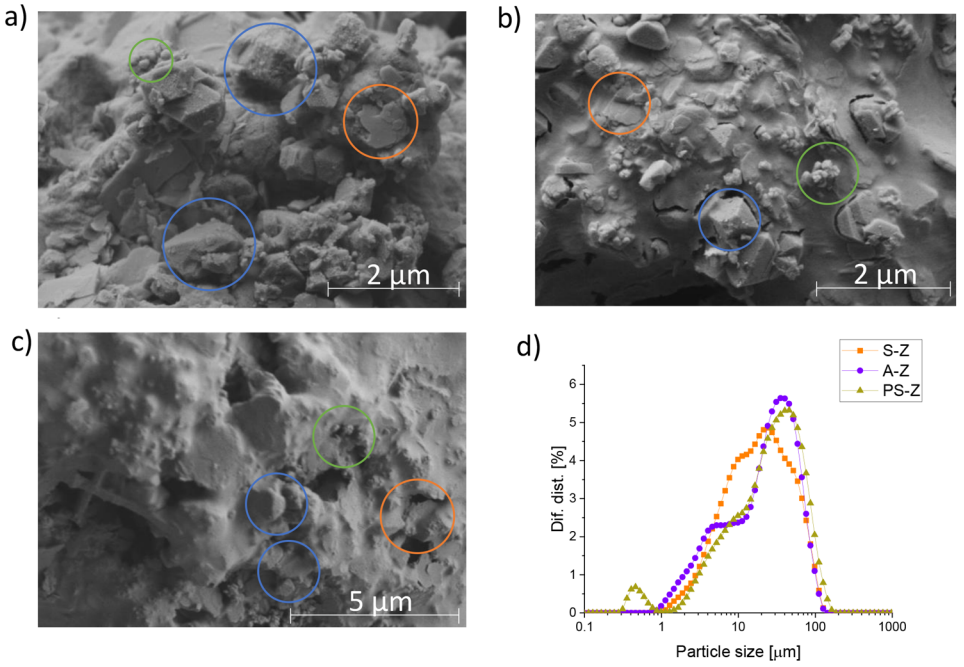

Figure 6. SEM pictures of the composites (a) S-Z and (b) A-Z (magnification factor: ×20 000) and (c) SEM picture of PS-Z (magnification factor: ×10 000) with zeolite Y observed in the blue circles, ZSM-5 in the green circles, and kaolin in the orange circles. (d) Particle size distribution of composites.

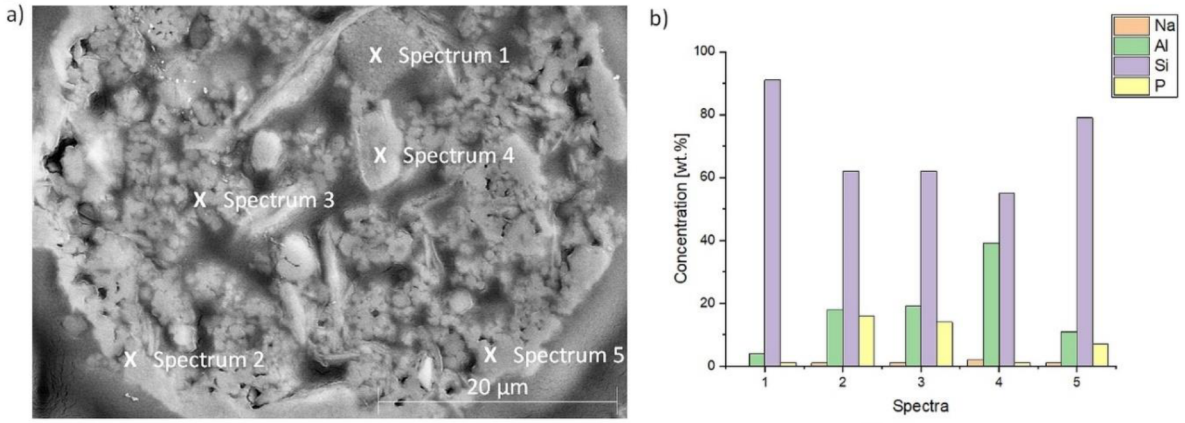

Figure 7. EDX results for composite with AlPO binder (PS-Z): (a) SEM picture of PS-Z and (b) EDX results of PS-Z.

the presence of phosphates during the sample preparation. Ion exchange can remove the aluminum species, which cover the acid sites of the zeolite. In addition, it removes most of the residual sodium from LUDOX in the binder. Therefore, an ion exchange was performed for all samples in order to reactivate the acid sites of the composites. Because of different pore sizes and surface acidity properties, the formed composites possess different catalytic characteristics for the cracking reaction of hexanes. In all cases, the catalyst samples showed a high conversion at the start of the measurement, which decreased steadily up to a conversion of 20% (see Figure 5). This kind of deactivation is mainly attributed to coke formation, which is observed in catalytic tests. In the formulation with water glass binder (S), the formation of olefins was reduced because of the low acidity of the matrix; that is, all the cracking reactions occur mainly at the zeolite Y, where hydrogen transfer takes place because of the low Si/Al ratio of the zeolite.[40] In addition, as observed in Figure 4 and Table 3, the pore volume of this sample was low, which reduced the pore diffusion in the system. This favored subsequent cracking reactions because of diffusion limitations and reduced the yield of olefins.[41] In addition, sample A showed no significant differences in the conversion and the olefin yield in comparison to those of sample S. This is attributed to the similar acidity of these samples. A different situation was observed for the PS formulation, which showed a lower conversion of hexanes. However, the olefin yield was similar to that of the other samples, although the acidity was reduced, which is a consequence of the reduction of external acid sites.[42]

Constraint index (CI) was also calculated for these samples. The constraint index indicates the state of the pores and the shape selectivity of the zeolites in the catalyst. A CI value below one indicates the dominance of wide pores as for zeolite Y (12-membered rings) and external acid sites, which favor the conversion of branched molecules. At CI values between 1 and 12, there is dominance of medium pore shapes as in zeolite ZSM-5 (10-membered rings). CI values greater than 12 indicate

https://doi.org/10.1021/acsomega.2c00446
ACS Omega 2022, 7, 16430−16441

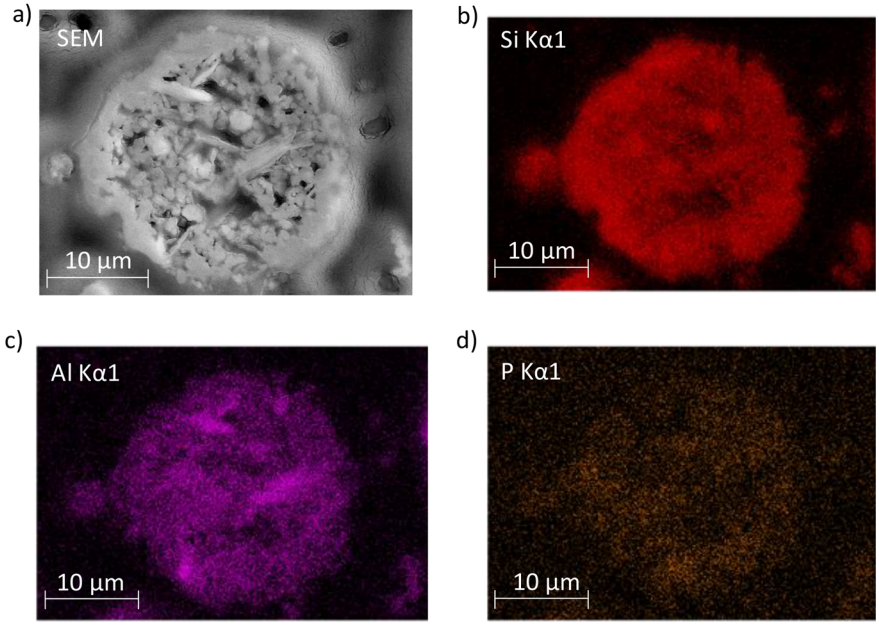

Figure 8. SEM images and EDX mapping of sample PS-Z in epoxy resin: (a) SEM image (magnification factor: 3000); (b) silicon mapping; (c) aluminum mapping; and (d) phosphorus mapping.

preferred cracking at narrow pores (8-membered rings) which favor the conversion of linear hydrocarbons.[16,43]

For the samples, an increment of the index with time was observed because of the narrowing of the particle pores by coke formation. In the case of sample S, the constraint index reached the value of CI = 1 because of the deactivation. However, the constraint index maintained a value CI < 1 for the other formulations, which indicates that the pores of the particle are wide and accessible. This leads to more selective cracking of branched 3-methylpentane than *n*-hexane (see Figure 5). Sample A showed wider pores at the beginning of the measurement, which were covered faster than in the case of PS, where the pores maintained their diameter during the experiment. At the end of the experiment, the sample PS had wider pores compared to the others, as already deduced from morphological analysis (see Table 3).

3.2. Addition of ZSM-5. In this experimental series, ZSM-5 was added to the spray drying slurry. Presence of ZSM-5 crystals was confirmed via SEM (see Figures 1 and 6). ZSM-5 crystals are distributed over the particle surface. From laser scattering results the average particle size is again in the range of the spray nozzle diameter (approximately 20−25 μm). Compared to the formulation without ZSM-5, only the composite with phosphates and colloidal silica PS-Z shows a higher average particle size (see Table 3). This can be attributed to the contribution of the ZSM-5 crystals, which are located on the external surface. The smaller crystals tend to form more stable and bulkier agglomerates with the phosphate and silica binder, which promotes the formation of an external particle shell.

EDX analysis was used to confirm a binder accumulation within the external particle crust for the sample PS-Z (see Figure 7). For this analysis, a composite was cut sectionally, in order to observe its internal morphology. The SEM picture indicates that the binder forms a porous layer around the grain. Under the surface, the components are bound and form pores of different geometry, which are favorable for transport processes during the catalytic cracking reaction. In order to observe the elementary composition of these components in more detail, EDX measurements were performed as well. Five different spectra were taken for this analysis. Spectrum 1 corresponds to zeolite Y. Spectra 2, 3, and 5 are in the binder phase, and spectrum 4 is related to kaolin. According to the EDX results (see Figure 7), the binder phase is rich in silicon and phosphorus, as also observed in the ICP-OES measurement (see Table 2). In addition, these elements are observed in the surface layer, which confirms the formation of a particle crust from the binder. Moreover, sodium impurities are present in this formulation, because it is detected in all the spectra. However, it is slightly more concentrated in the internal zone of the particle (Figure 7, spectrum 4). These small sodium residues could not be separated from the composite during the ion exchange treatment because penetration of ammonium nitrate solution to composite grains becomes less efficient for bigger particles.

For visualization of the elementary distribution over the PS-Z particle (see Figure 8), an EDX mapping was performed. The results confirm that silicon and phosphorus are more present in the surface, which corresponds to the binder. In addition, internal spots rich in silicon are observed in the particle. These spots correspond to the zeolite Y because of its Si/Al ratio. Furthermore, aluminum-rich zones are observed in the composite, which correspond to the kaolin phase.

A deeper look into the phase distribution of final grains from X-ray diffraction confirms again a reflection pattern of zeolite Y (see Figure 9), and small signals of ZSM-5 also exist. No further phases can be identified by XRD. Reference for this analysis was the commercial HY CBV 400 and ZSM-5 CBV 5544G by Zeolyst, which are comparable with references from the literature[19,44] (see Figure S1).

In addition to SEM imaging, the surface morphology was also analyzed by physisorption of nitrogen (see Figure 10a), and the mesopore distribution was also determined by the BJH method. The adsorption isotherms of the samples are of the type II, which is typical for samples with micropores and large pores. Furthermore, the sample A-Z shows a transition to isotherm type IV(a), which is indicative of smaller macropores or even mesopores.[20,21] (For further details, see Figure S2.) In addition,

https://doi.org/10.1021/acsomega.2c00446
ACS Omega 2022, 7, 16430−16441

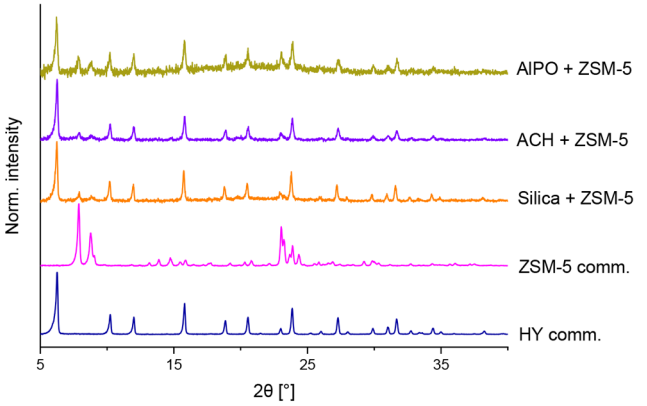

Figure 9. XRD patterns of formulated samples with ZSM-5 and different binders. Reference for zeolite Y and ZSM-5: commercial Zeolyst.

the distribution results show the presence of mesopores between 4 and 10 nm. However, tensile strength effect is observed again. In comparison to the formulations without ZSM-5, there is no significant change in the pore size distribution and the specific surface area for the samples S-Z and PS-Z. Only a slight increment of these parameters is detected for the sample A-Z (see Figure 10a).

Surface acidity was determined for these samples by TPAD. A deeper look on ammonia desorption experiments reveals that the addition of acidic H-ZSM-5 enhances the acidity of the samples. Moreover, the formulations with aluminum-based binders (A-Z and PS-Z) show clearly a higher amount of ammonia in desorption experiments than the S-Z formulation.

This indicates that the additive (zeolite ZSM-5) is well distributed and accessible over the surface of the composite material. The consequence of these morphologic characteristics and higher total acidity is the enhancement of the cracking conversion, which is illustrated as the increment of the conversion of *n*-hexane and 3-methylpentane (see Figure 11). The produced samples maintain a high conversion value over the complete measurement time (6 h on stream), and the deactivation is less harsh compared to the samples without ZSM-5. Moreover, the enhancement effect of the ZSM-5 is the highest in the PS-Z formulation for linear hydrocarbons, although the acidity of this sample is lower than the A-Z formulation. This is explained by the type of pores and the distribution of ZSM-5 within the final composite grains. The A-Z sample possesses wider pores than PS-Z. This reduces the reactivity of the phosphate formulation for branched hydrocarbons in contrast to linear hydrocarbons. Moreover, SEM images indicate a certain amount of ZSM-5 distributed on the external surface of the particle crust of sample PS-Z. Both are in line with the constraint index of these samples, which is higher for sample PS-Z than for A-Z. In addition, the constraint index of both samples is higher than that of the samples without ZSM-5 (see Figure 11c). In all cases, the constraint index of the samples is greater than one, which implies the presence of narrow pores of ZSM-5 and a more selective conversion of linear over branched hydrocarbons.

Coke is also formed in the catalyst samples after 6 h on stream (see Figure 12). It is produced by the hydrogen-transfer reactions, which are typical for the zeolite Y. The coke formation is the main deactivation mechanism in this system, because coke covers the pore surface and reduces the contact of the active sites with the reactants. This is observed by a drop in hexanes conversion for each sample (see Figures 5 and 11). However, this deactivation mechanism depends on the porosity and the zeolite type used in the formulation. The analysis of the coke formed in the process was done twice by TGA with a heating rate of 3 and 10 K min^{-1} (see also Figure S4), as well as DTG analysis obtained from these data. The profile of the DTG curves (see Figure 12) is similar for both heating rates and all the samples, which shows that the coke species formed in the reaction have a similar nature in all cases.[45] The main difference among the samples is the coke amount produced in the reaction. In the case of the formulations with ZSM-5 (*-Z), the deactivation tendency in hexane cracking and the total amount of coke after the tests are lower because of the reduced selectivity of ZSM-5 for coke in comparison to zeolite Y.[34] From CI results, it can be established that the binder does not selectively modify some inner pore structures of the zeolite. In addition, different coking behavior is mainly defined by the transport through the composite grain to the interface with the zeolite (diffusion). In the case of facilitated transport, *e.g.*, in the case of the spray product with phosphate-silica binder, the wider pores allow the formation and fast release of bigger aromatic molecules, which do not contribute to the production of coke. Therefore, the additive used and the pore type in the composite determine the coke formation in the reaction. This aspect can increase the lifespan of the catalyst, if mesopores and additional highly active and low-coking additives are present. The less coke-selective catalysts require less regeneration cycles, while each cycle reduces their catalytic activity because of (hydro-)thermal deactivation and mechanical attrition.

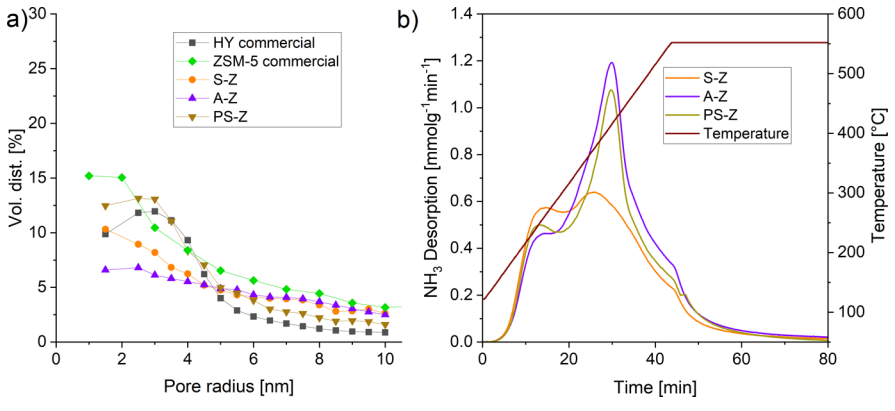

Figure 10. (a) Pore size distribution by BJH theory. (b) TPAD results of composites with ZSM-5 using different binders.

https://doi.org/10.1021/acsomega.2c00446
ACS Omega 2022, 7, 16430−16441

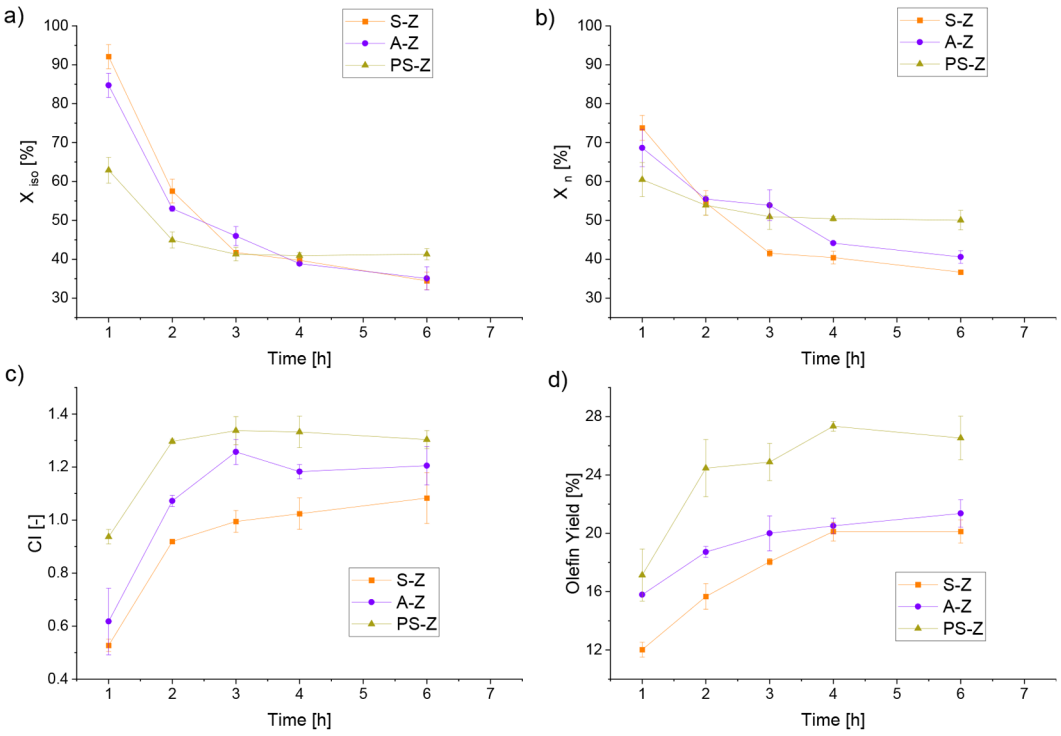

Figure 11. Conversion of (a) 3-methylpentane and (b) *n*-hexane for each formulation using ZSM-5 and different binders. (c) Constraint index and (d) olefin yield of formulated catalysts with ZSM-5 and different binders.

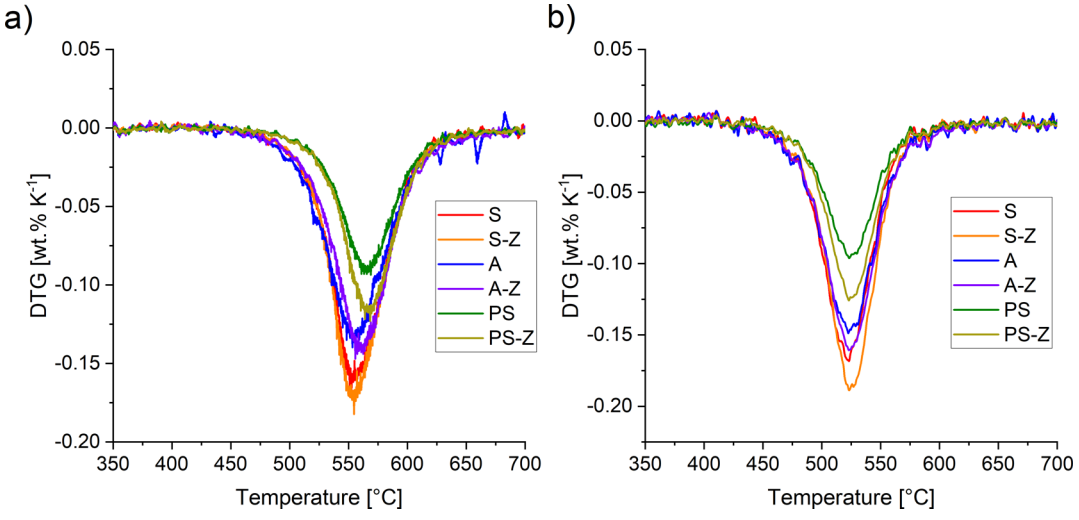

Figure 12. DTG results derived from thermogravimetric analysis with a heating rate of (a) 10 K min^{-1} and (b) 3 K min^{-1}.

Another important benefit of the composites PS- and PS-Z is their high selectivity for olefins. This parameter depends on the residence time of the reactants in the catalyst particle surface, which is defined by the porosity and the size of zeolite crystals in the particle.[40,46] For all binder experiments, the addition of ZSM-5 increases the formation of olefins in the reaction (see Figure 11d). Because of the smaller pore radius of ZSM-5, the hydrogen-transfer reaction is limited,[23] and so the production of olefins is favored. In addition, their smaller zeolite crystals are ideal for olefin production because of a lower residence time. Thus, their selectivity toward formation of small olefins rises. This effect is enhanced in the case of sample PS-Z through reduction of the amount of strong acid sites (see Figure 10), which are also considered to partially promote hydrogen-transfer reactions and fast coke formation.[38,47]

4. CONCLUSION

The selection of the components in the formulation of cracking catalysts is an important aspect to determine the activity, selectivity, and even the durability in the process. Basically, the catalytic properties of a catalyst strongly depend on its morphology, which is defined by the used binder and additive in the formulation. Primarily, binders determine the porosity of the matrix, *e.g.*, water glass produces matrixes with low porosity. This contributes to a quick deactivation by coke and unselective cracking, which is confirmed by the constraint index. Furthermore, hydrogen-transfer reactions are dominant with

https://doi.org/10.1021/acsomega.2c00446
ACS Omega 2022, 7, 16430−16441

this less active silica matrix, and the coke formation is enhanced. In addition, aluminum chloride derived matrixes deactivate as well, as observed by the constraint index. However, the formed matrix increases the activity of the shaped particle but does not alter the selectivity to olefins. Beside this, aluminum phosphate together with colloidal silica is less acidic than the aluminum chloride derived matrix, but it produces stable wide pores, an external crust of the grain, and calmed down or blocked (external) sites, which reduce the fast pore blocking from coke formation. In addition to the binder selection, additives contribute with their catalytic properties to the final grain. In the case of ZSM-5, the constraint index indicates the introduction of narrow pores as known from the MFI-type pore structure. Consequently, the production of olefins is enhanced and coking is reduced by the shape-selective prevention of bigger aromatic coke precursors compared to zeolite Y as the only zeolite component. The formulation method used in this work ensures the production of different porous active composites. In particular, combined aluminum phosphate and silica-containing slurries together with ZSM-5 produce highly porous and medium acidic composites which enhance the olefins yield at low deactivation rate.

■ ASSOCIATED CONTENT

Supporting Information

The Supporting Information is available free of charge at https://pubs.acs.org/doi/10.1021/acsomega.2c00446.

XRD reflections of reference materials (Figure S1); adsorption isotherms of samples analyzed in the work (Figure S2); dependency between ion exchange of the composites and hexane cracking (Figure S3); TGA analysis at 10 and 3 K min^{-1} (Figure S4) (PDF)

■ AUTHOR INFORMATION

Corresponding Author

Jan J. Weigand − *Faculty of Chemistry and Food Chemistry, Chair of Inorganic Molecular Chemistry, Technische Universität Dresden, 01069 Dresden, Germany;* orcid.org/0000-0001-7323-7816; Email: jan.weigand@tu-dresden.de

Authors

Andres Carrasco Saavedra − *Faculty of Chemistry and Food Chemistry, Chair of Inorganic Molecular Chemistry, Technische Universität Dresden, 01069 Dresden, Germany*

Vladislav Timoshev − *Faculty of Chemistry and Food Chemistry, Chair of Inorganic Molecular Chemistry, Technische Universität Dresden, 01069 Dresden, Germany*

Mathias Hauck − *Faculty of Chemistry and Food Chemistry, Chair of Inorganic Molecular Chemistry, Technische Universität Dresden, 01069 Dresden, Germany*

Mehdi Hassan Nejad − *Aiotec GmbH, 13507 Berlin, Germany*

Tung Thanh Dang − *Vietnam National Oil and Gas Group, Hanoi City 118000, Vietnam*

Xuan Hoan Vu − *Vietnam Petroleum Institute, Hanoi City 122000, Vietnam;* orcid.org/0000-0001-9529-8716

Markus Seifert − *Faculty of Chemistry and Food Chemistry, Chair of Inorganic Molecular Chemistry, Technische Universität Dresden, 01069 Dresden, Germany*

Oliver Busse − *Faculty of Chemistry and Food Chemistry, Chair of Inorganic Molecular Chemistry, Technische Universität Dresden, 01069 Dresden, Germany*

Complete contact information is available at: https://pubs.acs.org/10.1021/acsomega.2c00446

Author Contributions

A.C.S. elaborated the concept of this work, the sample preparation including analysis and discussion. V.T. elaborated a concept for the performed catalytic testing, including analysis and discussion; surface, particle, and acidity characterization; and ICP-OES elementary analysis. M.H. conceptualized the synthesis of aluminum chloride binder and did proofreading. M.S. established guidance for conceptualization, characterization, catalytic testing, discussion, performed the SEM and EDX measurements with formal analysis, and did proofreading and contributed to supervision of the project. M.H., X.H.V., and T.T.D. reviewed this work including formal and content-related correction. O.B. contributed for discussion of results, internal revision (proofreading), did administration of resources and supervision of the project. J.J.W. was the main supervisor and reviewer of the work, as well as head of funding acquisition and resource management.

Notes

The authors declare no competing financial interest.

■ ACKNOWLEDGMENTS

The authors thank the German Federal Ministry for Education and Research (BMBF) for financial funding of this research within the directive Client-II "International Partnerships for Sustainable Innovation" by FONA^3 (ReCaLl Project, funding code: 033R188A). Special thanks goes to Prof. M. Ruck and Prof. T. Doert (TU Dresden) for access to XRD, SEM and EDX infrastructure.

■ REFERENCES

(1) Corma, A.; Corresa, E.; Mathieu, Y.; Sauvanaud, L.; Al-Bogami, S.; Al-Ghrami, M. S.; Bourane, A. Crude oil to chemicals: light olefins from crude oil. *Catal. Sci. Technol.* **2017**, *7*, 12−46.

(2) Buurmans, I. L. C.; Ruiz-Martínez, J.; Knowles, W. V.; van der Beek, D.; Bergwerff, J. A.; Vogt, E. T. C.; Weckhuysen, B. M. Catalytic activity in individual cracking catalyst particles imaged throughout different life stages by selective staining. *Nat. Chem.* **2011**, *3*, 862−867.

(3) Harding, R.; Peters, A.; Nee, J. New developments in FCC catalyst technology. *Appl. Catal., A* **2001**, *221*, 389−396.

(4) Rawlence, D. J.; Gosling, K. FCC catalyst performance evaluation. *Appl. Catal.* **1988**, *43*, 213−237.

(5) Vogt, E. T. C.; Weckhuysen, B. M. Fluid catalytic cracking: recent developments on the grand old lady of zeolite catalysis. *Chem. Soc. Rev.* **2015**, *44*, 7342−7370.

(6) Woltermann, G.; Magee, J.; Griffith, S. *Fluid Catalytic Cracking: Science and Technology*; Magee, J. S., Mitchell, M. M., Eds.; Elsevier Science Publishers B.V.: Amsterdam, 1993; pp 106−125.

(7) Hargreaves, J. S. J.; Munnoch, A. L. A survey of the influence of binders in zeolite catalysis. *Catal. Sci. Technol.* **2013**, *3*, 1165.

(8) Thomas, J. M.; Thomas, W. *Principles and Practice of Heterogeneous Catalysis*, 2nd ed.; Thomas, J., Thomas, W., Eds.; Wiley-VCH: Weinheim, 2015; pp 15−16.

(9) Sadeghbeigi, R. *Fluid catalytic cracking handbook*, 4th ed.; Sadeghbeigi, R., Ed.; Elsevier: Cambridge, 2020; pp 90−92.

(10) Carpenter, J. R.; Yeh, S.; Zones, S. I.; Davis, M. E. Further investigations on Constraint Index testing of zeolites that contain cages. *J. Catal.* **2010**, *269*, 64−70.

(11) Al-Khattaf, S. The Influence of Alumina on the Performance of FCC Catalysts during Hydrotreated VGO Catalytic Cracking. *Energy Fuels* **2003**, *17*, 62−68.

(12) Carrasco Saavedra, A.; Seifert, M.; Hauck, M.; Brünner, A.; Doert, T.; Busse, O.; Weigand, J. J. Peptization Control of Aluminum

Chloride-Containing Composites for Catalysts with Active Matrix. *Chem. Eng. Technol.* **2021**, *44*, 1051−1057.
(13) Dollimore, D.; Spooner, P.; Turner, A. The BET method of analysis of gas adsorption data and its relevance to the calculation of surface areas. *Surf. Technol.* **1976**, *4*, 121−160.
(14) Barrett, E. P.; Joyner, L. G.; Halenda, P. P. The Determination of Pore Volume and Area Distributions in Porous Substances. I. Computations from Nitrogen Isotherms. *J. Am. Chem. Soc.* **1951**, *73*, 373−380.
(15) Joyner, L. G.; Barrett, E. P.; Skold, R. The Determination of Pore Volume and Area Distributions in Porous Substances. II. Comparison between Nitrogen Isotherm and Mercury Porosimeter Methods. *J. Am. Chem. Soc.* **1951**, *73*, 3155−3158.
(16) Weitkamp, J.; Ernst, S. Probing the shape selective properties of zeolites by catalytic hydrocarbon reactions. *Catal. Today* **1988**, *3*, 451−457.
(17) American Society for Testing of Materials. Standard Test Method for Determination of Individual Components in Spark Ignition Engine Fuels by 100−Metre Capillary (with Precolumn) High-Resolution Gas Chromatography; 2019.
(18) Carrasco Saavedra, A.; Seifert, M.; Hannß, M.; Henle, T.; Lê-Anh, M.; Busse, O.; Weigand, J. J. Peptization Control of Composite Materials Containing Water Glass for Spray Drying of Catalysts. *Chem. Eng. Technol.* **2021**, *44*, 732−740.
(19) Parise, J. B.; Corbin, D. R.; Abrams, L.; et al. Structure of Dealuminated Linde Y-Zeolite; Si139.7 Al52.3 O384 and Si173.1 Al18.9 O384: Presence of Non-framework Al Species. *Acta Crystallogr.* **1984**, *40*, 1493−1497.
(20) Pidko, E.; Hensen, E. *Catalysis*; Beller, M., Renken, A., van Santen, R., Eds.; Wiley-VCH: Weinheim, 2012; pp 517−519.
(21) Thommes, M.; Kaneko, K.; Neimark, A. V.; Olivier, J. P.; Rodriguez-Reinoso, F.; Rouquerol, J.; Sing, K. S. Physisorption of gases, with special reference to the evaluation of surface area and pore size distribution (IUPAC Technical Report). *Pure Appl. Chem.* **2015**, *87*, 1051−1069.
(22) Groen, J. C.; Peffer, L. A.; Pérez-Ramírez, J. Pore size determination in modified micro- and mesoporous materials. Pitfalls and limitations in gas adsorption data analysis. *Microporous Mesoporous Mater.* **2003**, *60*, 1−17.
(23) De Lange, M. F.; Vlugt, T. J.; Gascon, J.; Kapteijn, F. Adsorptive characterization of porous solids: Error analysis guides the way. *Microporous Mesoporous Mater.* **2014**, *200*, 199−215.
(24) van der Bij, H. E.; Weckhuysen, B. M. Phosphorus promotion and poisoning in zeolite-based materials: synthesis, characterisation and catalysis. *Chem. Soc. Rev.* **2015**, *44*, 7406−7428.
(25) Plitt, L. R.; Kawatra, S. K. Estimating the cut (d50) size of classifiers without product particle-size measurement. *Int. J. Miner. Process.* **1979**, *5*, 369−378.
(26) Eremin, Y. A. *Encyclopedia of Modern Optics*; Guenther, R. D., Ed.; Elsevier: Oxford, 2005; pp 326−330.
(27) Gorte, R. J.; Crossley, S. P. A perspective on catalysis in solid acids. *J. Catal.* **2019**, *375*, 524−530.
(28) Yi, X.; Liu, K.; Chen, W.; Li, J.; Xu, S.; Li, C.; Xiao, Y.; Liu, H.; Guo, X.; Liu, S.-B.; Zheng, A. Origin and Structural Characteristics of Tri-coordinated Extra-framework Aluminum Species in Dealuminated Zeolites. *J. Am. Chem. Soc.* **2018**, *140*, 10764−10774.
(29) de Lucas, A.; Valverde, J. L.; Sánchez, P.; Dorado, F.; Ramos, M. J. Influence of the Binder on the n -Octane Hydroisomerization over Palladium-Containing Zeolite Catalysts. *Ind. Eng. Chem. Res.* **2004**, *43*, 8217−8225.
(30) Hashiba, T.; Hayashi, D.; Katada, N.; Niwa, M. Decrease of catalytic activity and solid acidity by ion exchange of Na cation on HZSM-5. *Catal. Today* **2004**, *97*, 35−39.
(31) Fougerit, J. M.; Gnep, N. S.; Guisnet, M.; Amigues, P.; Duplan, J. L.; Hugues, F. Zeolites and Related Microporous Materials: State of the Art 1994 - Proceedings of the 10th International Zeolite Conference, Garmisch-Partenkirchen, Germany, 17−22 July 1994; Studies in Surface Science and Catalysis. Effect of the binder on the properties of a mordenite catalyst for the selective conversion of methanol into light olefins; Elsevier, 1994; pp 1723−1730.
(32) Misk, M.; Joly, G.; Magnoux, P.; Guisnet, M.; Jullian, S. Formation of coke from propene over 5A adsorbents − influence of the binder on the coke composition, location and removal. *Microporous Mesoporous Mater.* **2000**, *40*, 197−204.
(33) Sohn, J. R.; DeCanio, S. J.; Fritz, P. O.; Lunsford, J. H. Acid catalysis by dealuminated zeolite Y. 2. The roles of aluminum. *J. Phys. Chem.* **1986**, *90*, 4847−4851.
(34) Cerqueira, H. S.; Caeiro, G.; Costa, L.; Ramôa Ribeiro, F. Deactivation of FCC catalysts. *J. Mol. Catal. A: Chem.* **2008**, *292*, 1−13.
(35) Zheng, Y.; Song, J.; Xu, X.; He, M.; Wang, Q.; Yan, L. Peptization Mechanism of Boehmite and Its Effect on the Preparation of a Fluid Catalytic Cracking Catalyst. *Ind. Eng. Chem. Res.* **2014**, *53*, 10029−10034.
(36) Michels, N.-L.; Mitchell, S.; Pérez-Ramírez, J. Effects of Binders on the Performance of Shaped Hierarchical MFI Zeolites in Methanol-to-Hydrocarbons. *ACS Catal.* **2014**, *4*, 2409−2417.
(37) Lercher, J. A.; Jentys, A.; Brait, A. *Acidity and Basicity; Molecular Sieves. Catalytic Test Reactions for Probing the Acidity and Basicity of Zeolites*; Springer: Berlin, 2008; pp 153−212.
(38) Lee, K.-Y.; Lee, H.-K.; Ihm, S.-K. Influence of Catalyst Binders on the Acidity and Catalytic Performance of HZSM-5 Zeolites for Methanol-to-Propylene (MTP) Process: Single and Binary Binder System. *Top. Catal.* **2010**, *53*, 247−253.
(39) Saka, Y.; Chiyoda, N.; Watanabe, K. Effect of Catalytic Stability Enhancement with Mono Aluminum Phosphate and Performance in Commercial FCC Unit. *J. Jpn. Petrol. Inst.* **2015**, *58*, 285−292.
(40) Bari Siddiqui, M. A.; Aitani, A. M.; Saeed, M. R.; Al-Khattaf, S. Enhancing the Production of Light Olefins by Catalytic Cracking of FCC Naphtha over Mesoporous ZSM-5 Catalyst. *Top. Catal.* **2010**, *53*, 1387−1393.
(41) Holland, B. T.; Subramani, V.; Gangwal, S. K. Utilizing Colloidal Silica and Aluminum-Doped Colloidal Silica as a Binder in FCC Catalysts: Effects on Porosity, Acidity, and Microactivity. *Ind. Eng. Chem. Res.* **2007**, *46*, 4486−4496.
(42) Zhang, X.; Cheng, D.; Chen, F.; Zhan, X. The Role of External Acidity of Hierarchical ZSM-5 Zeolites in n -Heptane Catalytic Cracking. *ChemCatChem.* **2018**, *10*, 2655−2663.
(43) Frillette, V. J.; Haag, W. O.; Lago, R. M. Catalysis by crystalline aluminosilicates: Characterization of intermediate pore-size zeolites by the "Constraint Index. *J. Catal.* **1981**, *67*, 218−222.
(44) Baerlocher, C.; McCusker, L. B.; Olson, D. H. *Atlas of zeolite framework types*, 6th rev. ed.; Baerlocher, C., McCusker, L. B., Olson, D. H., Eds.; Elsevier: Amsterdam, 2007; pp 213−214.
(45) Däumer, D.; Räuchle, K.; Reschetilowski, W. Experimental and Computational Investigations of the Deactivation of H-ZSM-5 Zeolite by Coking in the Conversion of Ethanol into Hydrocarbons. *ChemCatChem.* **2012**, *4*, 802−814.
(46) Buchanan, J. The chemistry of olefins production by ZSM-5 addition to catalytic cracking units. *Catal. Today* **2000**, *55*, 207−212.
(47) Awayssa, O.; Al-Yassir, N.; Aitani, A.; Al-Khattaf, S. Modified HZSM-5 as FCC additive for enhancing light olefins yield from catalytic cracking of VGO. *Appl. Catal., A* **2014**, *477*, 172−183.

https://doi.org/10.1021/acsomega.2c00446
ACS Omega 2022, 7, 16430−16441